Supporting information for: Two-dimensional sum-frequency generation (2D SFG) reveals structure and dynamics of a surface-bound peptide

Jennifer E. Laaser,[†] David R. Skoff,[†] Jia-Jung Ho,[†] Yongho Joo,[‡] Arnaldo L. Serrano,[†] Jay D. Steinkruger,[¶] Padma Gopalan,[‡] Samuel H. Gellman,[†] and Martin T. Zanni[*,†]

Department of Chemistry, University of Wisconsin-Madison, Madison, Wisconsin 53706, Department of Materials Science and Engineering, University of Wisconsin-Madison, Madison, Wisconsin 53706, and School of Environmental, Physical, and Applied Sciences, University of Central Missouri, Warrensburg, Missouri 64093

E-mail: zanni@chem.wisc.edu

CD, FTIR, and XPS Characterization of Peptide Samples

α-helical character of peptide AHP in solution

In Figure S1, we present circular dichroism (CD) spectrum of 46 μM AHP in 10 mM phosphate buffer in H_2O tuned to pH 7 with HCl and of 0.011 mM AHP in 24 mM MES buffer at pH 5. The double minima observed at 207 and 220 nm are characteristic of α-helical secondary structure. We

[*]To whom correspondence should be addressed
[†]University of Wisconsin-Madison
[‡]University of Wisconsin-Madison
[¶]University of Central Missouri

fit the CD spectrum at pH 7 and estimate that the peptide is approximately 50% helical in solution under these conditions.[1,2] Fitting the CD spectrum at pH 5 gave a similar estimate of helicity, but because of the lower signal-to-noise of the spectrum, due primarily to absorption in the MES buffer below 220 nm, fits were very sensitive to the fitting method and basis set used.

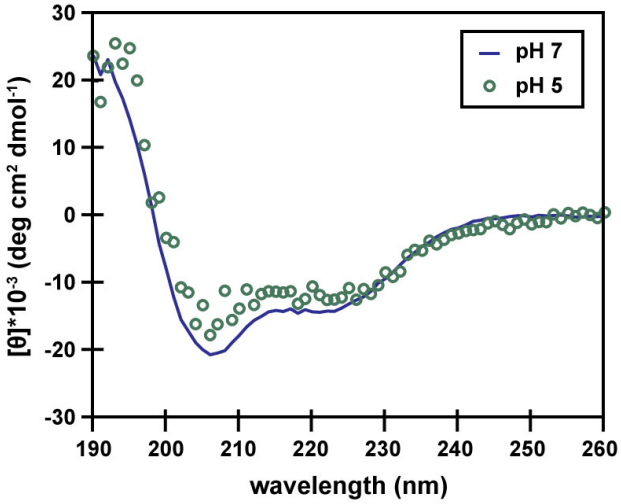

Figure S1: Circular dichroism spectrum of peptide AHP in D_2O, at pH 5 and pH 7.

The 2D IR spectra in the amide-I region shown in the main text were taken in 1 mM AHP in pH 7, 10 mM phosphate buffer prepared with D_2O. Limitations associated with the CD and 2D IR measurements prevent comparison of data obtained at a common concentration, but it seems reasonable to assume that the extensive helicity observed at the lower concentration necessary for CD analysis would be retained at higher concentration required for 2D IR. Association of peptide molecules driven by hydrophobic surface interactions, e.g. coiled coil formation, should be discouraged by intermolecular Coulombic repulsions between the carboxylates that flank the hydrophobic stripe;[3] however, any self-association that occurs at higher peptide concentrations should enhance the formation of α-helical secondary structure relative to the extent detected by CD at lower concentrations.

2D IR Spectra of AHP at pH 5

In Figure S2, we present 2D IR spectra of AHP in MES buffer at pH 5. The spectra are essentially

the same as those we report in the main text at pH 7, leading us to conclude that the secondary structure does not change substantially in this pH range.

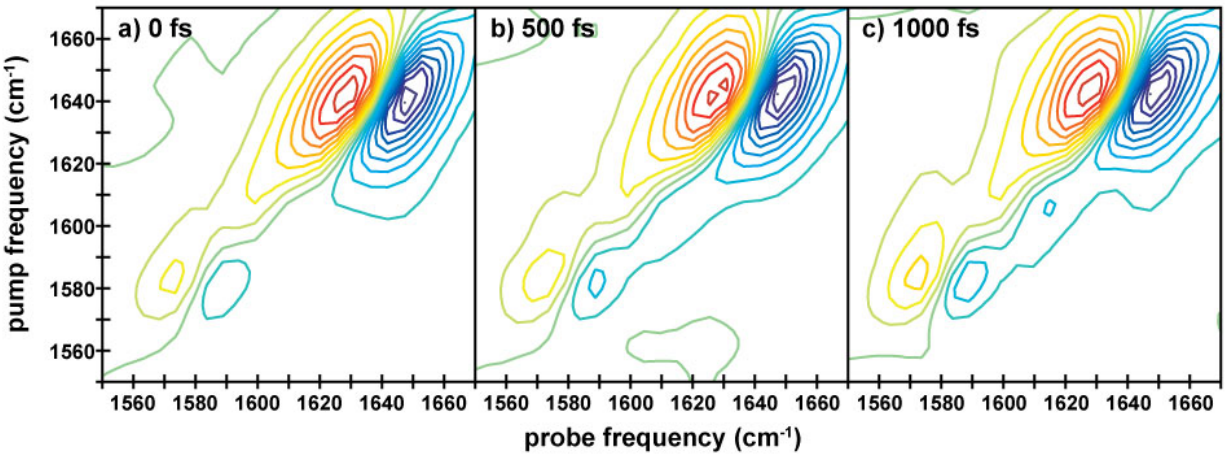

Figure S2: Two-dimensional infrared spectra of peptide AHP in MES buffer at pH 5, at waiting times of (a) t_2=0, (b) 500, and (c) 1000 fs.

Nodal slopes of α-helical peptides

In Figure S3, we include a 2D IR spectrum of $(AAAAK)_4AAAAY$ at 23°C in D_2O. This "AKA" peptide is strongly α-helical and serves as a reference spectrum.[4] The nodal line is tilted 28° from the vertical; tilts closer to 0° indicate more homogeneous lineshapes, while tilts closer to 45° indicate more inhomogeneous lineshapes.

Transmission and reflection FTIR

In Figure S4, we present a comparison between the bulk FTIR spectrum of peptide AHP in D_2O at pH 7 and the infrared reflection-absorption (IRRAS) spectrum of a monolayer of the peptide on a gold surface. The surface samples exhbit a distinct frequency shift for the main amide-I band, which shifts from 1642 to 1660 cm^{-1} upon dehydration and surface adsorption. Samples measured in D_2O also exhibit a -100 cm^{-1} shift in the amide-II band position relative to samples in H_2O. The 1660 cm^{-1} frequency is characteristic of the dehydrated peptide at the interface with the gold substrate.

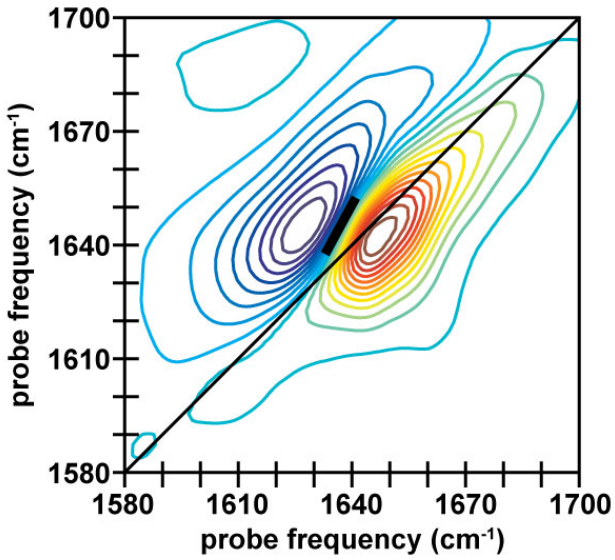

Figure S3: 2D IR spectrum of the AKA peptide at 23°C in D_2O

Estimate of Helix Tilt Angle

To estimate the tilt angle of the peptide helices from the surface normal, we used the ratio of the amide-I and amide-II responses from our FTIR spectra, as has been described previously.[5] The tilt angle is related to the ratio of the amide-I and amide-II responses by

$$\frac{I_I}{I_{II}} = c\frac{2\left[\frac{1}{2}(3\cos^2\gamma - 1)\right]\left[\frac{1}{2}(3\cos^2\theta_I - 1)\right] + 1}{2\left[\frac{1}{2}(3\cos^2\gamma - 1)\right]\left[\frac{1}{2}(3\cos^2\theta_{II} - 1)\right] + 1} \tag{S1}$$

where I_I and I_{II} are the intensities of the amide-I and amide-II bands, respectively; θ_I and θ_{II} are the tilt angles of the transition dipoles of these bands relative to the helix axis (chosen as 39° and 75°, respectively); γ is the tilt angle of the helix axis relative to the surface normal; and C is scaling factor reflecting the anisotropy of the system, which has a value of 1.5 as has been shown previously.[5]

Fitting our reflection FTIR spectra to two Lorentzians gives an intensity ratio of I_I/I_{II} = 1.96, which corresponds to a helix tilt angle of approximately 48° from the surface normal. The accuracy of this estimate is likely skewed by contributions from the arginine sidechains and the distribution of tilt angles in the monolayer, but this value is consistent with previously-reported tilt angles for self-assembled monolayers of thiol-bound helical peptides on gold, which typically range from 30

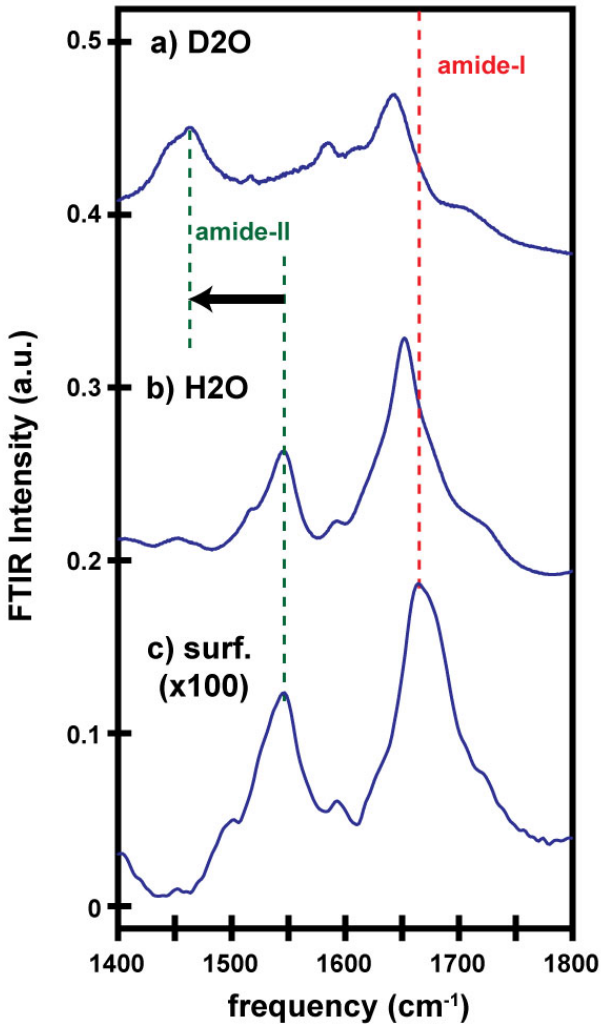

Figure S4: FTIR spectra of peptide AHP in (a) D_2O, (b) H_2O, and (c) on an Au surface, obtained in transmission and reflection experiments, respectively. The peak positions for the amide-I and amide-II bands are indicated by the red and green dotted lines, respectively.

to 60 degrees from the surface normal.[6]

Surface Coverage

In Figure S5 we provide XPS spectra obtained for our AHP monolayers on gold. The absolute elemental composition was determined by referencing the peak areas for C, O, S, and N to that for Au, which has a known atomic density.[7,8]

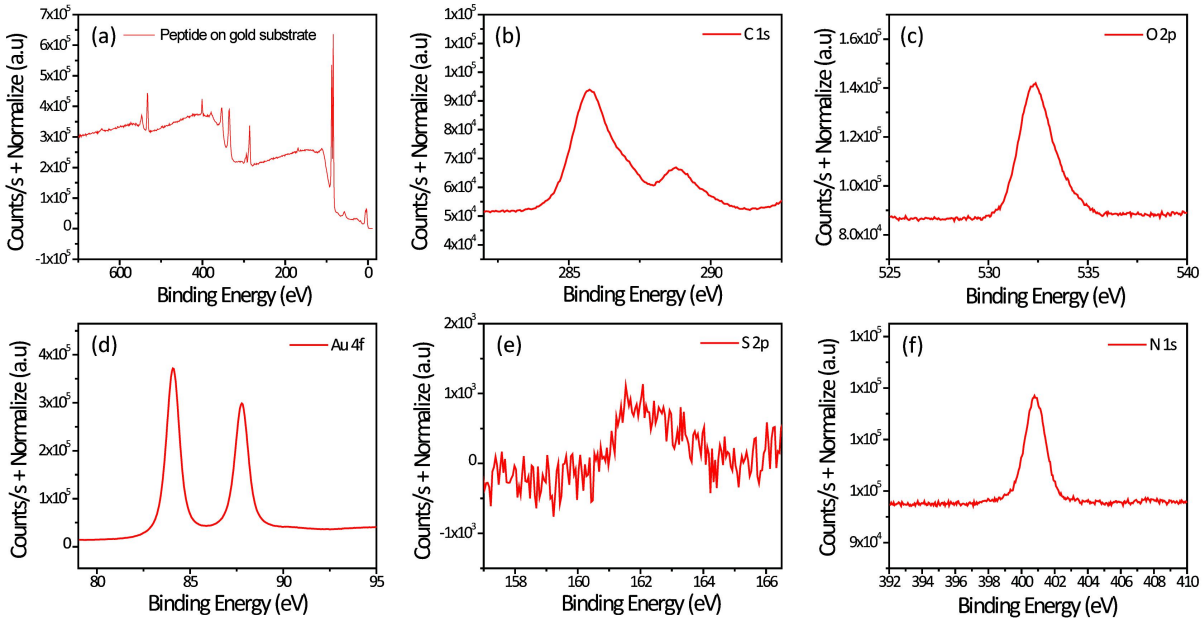

Figure S5: X-ray photoelectron spectroscopy (XPS) spectra of peptide on gold substrate. Representative survey (a), C(1s) (b), O(2p) (c), Au(4f) (d), S(2p) (e), and N(1p) (f) scans. For quantitative analysis an average of three spots on the substrate was measured.

Atomic coverages were calculated using the peak areas and sensitivity factors, and normalized by the number of oxygen (38), nitrogen (33), carbon (109), and sulfur (1) atoms present in the peptide. The resulting molecular coverages are given in Table S1.

Table S1: Coverage of peptide on Au substrate calculated from O(2p), C(1s), N(1s), and S(2p) peaks using Au(4f) peaks as internal standards

O(2p) (atoms/cm^2)	N(1s) (atoms/cm^2)	C(1s) (atoms/cm^2)	S(2p) (atoms/cm^2)	Average (molecules/c
2.71 ($\pm$0.12) x 10^{13}	2.52 ($\pm$0.26) x 10^{13}	3.52 ($\pm$0.07) x 10^{13}	4.10 ($\pm$0.25) x 10^{13}	3.21 ($\pm$0.22) x 10^{1}

The total average coverage is taken as the average of the coverage calculated from each measured element, though the numbers obtained from N(1s) and S(2p) are likely more representative of actual surface coverage as they are less sensitive to other organic contaminants on the surface.

Two-Dimensional Infrared and Sum Frequency Generation Spectroscopies

Our two-dimensional infrared and SFG experiments were similar to those we have described previously.[9,10] Three quarters of the 4 mJ/pulse output of regeneratively-amplified mode-locked Ti:Sapphire laser (Coherent Libra) was directed into an optical parametric amplifier followed by difference frequency generation in $AgGaS_2$ to generate up to 25 μJ/pulse of mid-IR light at 6 μm. The majority of the OPA/DFG output was directed into a Ge acousto-optic modulator-based pulse shaper to generate the E_1 and E_2 pump pulses for 2D experiments. For 2D IR experiments, the time delay of the E_1 pulse and the relative phase between the pulses was scanned on a shot-to-shot basis, as has been described previously.

For our 2D IR experiments, the shaped pump pulses were focused onto the sample using a 2 inch parabolic mirror. They were spatially and temporally overlapped with the fraction of the mid-IR not directed into the shaper, which we refer to as the probe. The transmitted probe was recollimated, focused into a 150 mm focal length polychromator, and detected on a 32-pixel MCT array. We scanned the t_1 delay between the E_1 and E_2 pump pulses from 0 to 3200 fs in 50 fs steps, with relative pump phases of 0 and π at each delay and a rotating frame frequency of 1450 cm^{-1}.

For our 2D SFG experiments, the fraction of the laser output not directed into the OPA was attenuated using a waveplate and polarizer, and was spectrally narrowed using a 1 nm FWHM interference filter, which in practice narrows the 800 nm pulse to a 20 or 25 cm^{-1} bandwidth. This 800 nm pulse was then overlapped with the mid-IR pump and probe pulses at the sample. The pulses were all p-polarized and had incidence angles of 65 and 70 degrees relative to the surface normal for the visible and mid IR pump/probe beams, respectively. The power of the visible pulse

was approximately 12 μJ at the sample. The signal was then recollimated, spectrally filtered to remove excess 800 nm light, and directed into a 320 mm focal length polychromator where it was disperssed by a 1200 groove/mm grating and detected on a thermoelectrically cooled CCD. Spectra for each pump pulse profile were averaged for 5 s and vertically binned on the CCD chip before being read out to the computer.

Unlike our previous 1D and 2D SFG experiments,[10,11] here we used the nonresonant signal from the gold substrates as an intrinsically phase-stabilized local oscillator. When using an 800 nm visible pulse for SFG, the absorptive part of the vibrational signal is to good approximation 90°out of phase with the nonresonant background,[12] so we applied a Fourier-filtering technique to retrieve the imaginary part of the spectrum in a similar manner as we have done to separate the rephasing and nonrephasing components of 2D SFG and 2D IR spectra in previous work.[10] We used a bare gold reference sample filtered in the same manner as a phase reference.

Calculation Details

Definition of the molecular response for a single amide-I unit

The molecular axes for an individual amide-I unit are defined such that the C(O)N bond lies in the molecular yz plane, with the CO bond tilted 34 degrees from the z axis, as shown in Figure S6.

In this frame, the transition dipole is defined as

$$\mu = \begin{pmatrix} 0 \\ -\sin\left(\frac{6.5\pi}{180}\right) \\ -\cos\left(\frac{6.5\pi}{180}\right) \end{pmatrix} \tag{S2}$$

such that it is oriented 27.5 degrees from the CO bond. This angle was chosen to ensure that the angle of a single amide-I transition dipole relative to the axis of a ideal α-helix was 42°, consistent with prior calculations.[13]

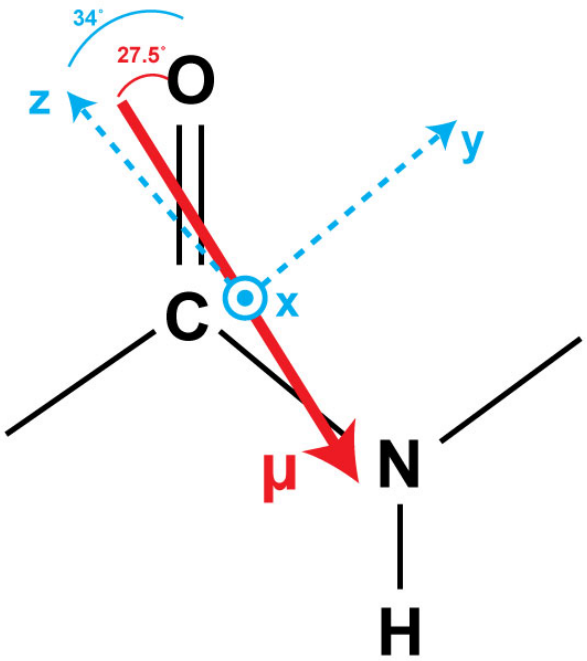

Figure S6: Diagram illustrating the orientation of the molecular response with respect to the amide-I bond. The red arrow indicates the direction and effective location of the transition dipole; the blue axes indicate the principle axes of the Raman polarizability.

The molecular-frame transition polarizability is defined as

$$\alpha = \begin{pmatrix} 0.25 & 0 & 0 \\ 0 & 1 & 0 \\ 0 & 0 & 5 \end{pmatrix} \tag{S3}$$

as reported in previous SFG studies on peptides.[13] Thus the chromophore is most polarizable along the molecular z-axis, 34 degrees from the CO bond, and least polarizable along the molecular x-axis, out of the plane of the C(O)N bond.

The "center", or effective position, of the vibrational mode is defined to be

$$\vec{r}_{amideI} = \vec{r}_C + 0.665\hat{r}_{CO} + 0.256\hat{r}_{CN} \tag{S4}$$

where $\vec{r}_C$ is the position of the carbon atom, $\hat{r}_{CO}$ is the unit vector along the CO bond, and $\hat{r}_{CN}$ is

the unit vector along the CN bond, with all positions given in Angstroms.[14] This position is used to calculate the distance between coupled modes, as necessary for the transition dipole coupling calculations described below.

Transition dipole coupling and two-exciton Hamiltonian model

For each C(O)N bond in the peptide structure, the single-residue response defined above was rotated and translated into the helix (or peptide) molecular frame, as described previously.[15] Once each local mode was rotated into the peptide frame, their couplings were calculated using the transition dipole coupling model,

$$\beta_{ij} = \frac{1}{4\pi\varepsilon_0}\left[\frac{\vec{\mu}_i \cdot \vec{\mu}_j}{r_{ij}^3} - 3\frac{(\vec{r}_{ij}\cdot\vec{\mu}_j)(\vec{r}_{ij}\cdot\vec{\mu}_j)}{r_{ij}^5}\right] \tag{S5}$$

where β_{ij} is the coupling between modes i and j, $\vec{\mu}_i$ and $\vec{\mu}_j$ are the transition dipoles of the two modes, and $\vec{r}_{ij}$ is the vector connecting the center position of the two modes.

We used this coupling model to construct a two-exciton Hamiltonian.[14] Under the harmonic approximation, we obtain the transition moments and coupling constants for the one- to two-exciton transitions by multiplying the the corresponding zero- to one-exciton transition moments by a factor of $\sqrt{2}$. Couplings between two-exciton states not sharing any local modes were set to zero.

After constructing the two-exciton Hamiltonian, we diagonalize the Hamiltonian to find the normal mode energies and the eigenvectors connecting the local modes with the normal modes. We calculate the normal mode transition dipoles by

$$\mu_N = \sum_n c_{Nn}\mu_n \tag{S6}$$

where μ_n is the transition dipole of the n^{th} local mode, μ_N is the transition dipole of the N^{th} normal mode, and the c_{Nn} are the coefficients of the eigenvectors connecting the local mode states to the N^{th} normal mode. The normal mode Raman tensors were calculated using an analogous formula

(replace μ with α). The normal mode hyperpolarizabilities β for each 2D response pathway were then calculated by taking the outer product of the transition moments:

$$\beta_{dcba} = \alpha_d \otimes \mu_c \otimes \mu_b \otimes \mu_a \tag{S7}$$

The normal mode hyperpolarizabilities were then rotated into the lab frame to calculate the lab-frame responses χ, as has been described previously.[15]

Random coil structure generation

The distribution of angles used to generate random coil structures is shown in Figure S7. The distribution was chosen to qualitatively match reported allowable ϕ,ψ angles for peptide structures.[16]

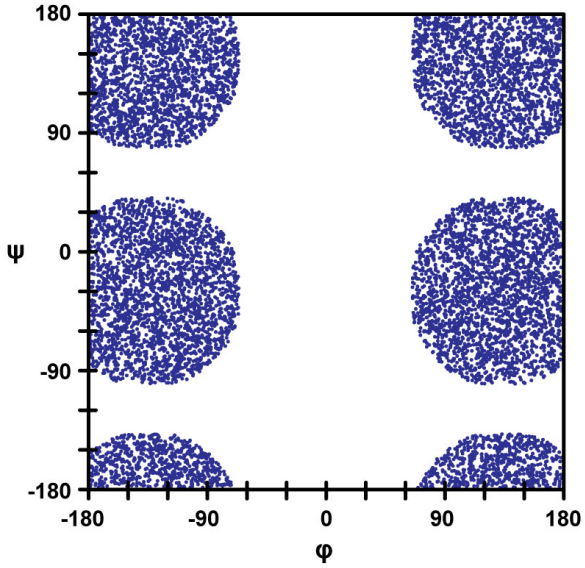

Figure S7: Ramachandran plot of distribution of ϕ,ψ angles used in calculation of disordered peptide structures.

The spectra in our helix/coil hybrids were simulated with a 20 cm^{-1} redshift in the frequency of the disordered residues to highlight the associated cross-peaks. We deleted one contour at 0 which was present in both the frequency-shifted and the un-shifted spectra.

References

(1) Greenfield, N. J. *Nature Protocols* **2007**, *1*, 2876–2890.

(2) Sreerama, N.; Woody, R. W. *Analytical Biochemistry* **2000**, *287*, 252–260.

(3) Woolfson, D. N. *Advances in Protein Chemistry* **2005**, *70*, 79–112.

(4) Grechko, M.; Zanni, M. T. *The Journal of Chemical Physics* **2012**, *137*, 184202.

(5) Miura, Y.; Kimura, S. *Langmuir* **1998**, *14*, 6935–6940.

(6) Kitagawa, K.; Morita, T.; Kimura, S. *Journal of Physical Chemistry B* **2004**, *108*, 15090–15095.

(7) Powell, C. J.; Jablonski, A. *Surface and Interface Analysis* **2000**, *29*, 108–114.

(8) Laibinis, P. E.; Bain, C. D.; Whitesides, G. M. *The Journal of Physical Chemistry* **1991**, *95*, 7017–7021.

(9) Middleton, C. T.; Woys, A. M.; Mukherjee, S.; Zanni, M. T. *Methods* **2010**, *52*, 12–22.

(10) Xiong, W.; Laaser, J. E.; Mehlenbacher, R. D.; Zanni, M. T. *Proceedings of the National Academy of Sciences of the United States of America* **2011**, *108*, 20902–20907.

(11) Laaser, J. E.; Xiong, W.; Zanni, M. T. *Journal of Physical Chemistry B* **2011**, *115*, 2536–2546.

(12) Potterton, E.; Bain, C. *Journal of Electroanalytical Chemistry* **1996**, *409*, 109–114.

(13) Nguyen, K. T.; Le Clair, S. V.; Ye, S.; Chen, Z. *Journal of Physical Chemistry B* **2009**, *113*, 12169–12180.

(14) Hamm, P.; Zanni, M. T. *Concepts and Methods of 2D Infrared Spectroscopy*, 1st ed.; Cambridge University Press, 2011; p 296.

(15) Laaser, J. E.; Zanni, M. T. *Journal of Physical Chemistry A* **2013**, *117*, 5875âĂŞ5890.

(16) Hu, H.; Elstner, M.; Hermans, J. *Proteins: Structure, Function, and Bioinformatics* **2003**, *50*, 451–463.